analytical chemistry

pubs.acs.org/ac

Article

# Isomer-Specific Two-Color Double-Resonance $IR^2MS^3$ Ion Spectroscopy Using a Single Laser: Application in the Identification of Novel Psychoactive Substances

Fred A. M. G. van Geenen,[⊥] Ruben F. Kranenburg,[⊥] Arian C. van Asten, Jonathan Martens, Jos Oomens, and Giel Berden*

Cite This: *Anal. Chem.* 2021, 93, 2687−2693

Read Online

ACCESS | Metrics & More | Article Recommendations | Supporting Information

**ABSTRACT:** The capability of an ion trap mass spectrometer to store ions for an arbitrary amount of time allows the use of a single infrared (IR) laser to perform two-color double resonance IR−IR spectroscopic experiments on mass-to-charge ($m/z$) selected ions. In this single-laser $IR^2MS^3$ scheme, one IR laser frequency is used to remove a selected set of isomers from the total trapped ion population and the second IR laser frequency, from the same laser, is used to record the IR spectrum of the remaining precursor ions. This yields isomer-specific vibrational spectra of the $m/z$-selected ions, which can reveal the structure and identity of the initially co-isolated isomeric species. The use of a single laser greatly reduces the experimental complexity of two-color $IR^2MS^3$ and enhances its application in fields employing analytical MS. In this work, we demonstrate the methodology by acquiring single-laser $IR^2MS^3$ spectra in a forensic context, identifying two previously unidentified isomeric novel psychoactive substances (NPS) from a sample that was confiscated by the Amsterdam Police.

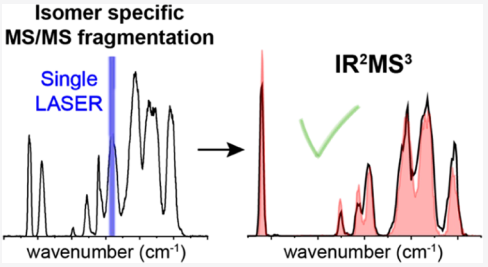


Infrared ion spectroscopy (IRIS) is a mass-spectrometry hyphenated method that provides detailed molecular structure information on mass-to-charge selected ions.[1−3] IRIS combines mass spectrometry (MS) with infrared (IR) laser spectroscopy to obtain a vibrational spectrum of ions inside a mass spectrometer. In this technique, ions are irradiated using a wavelength-tunable IR laser and the wavelength-dependent photodissociation yield is monitored. The vibrational spectrum can then be reconstructed from the relative intensities of precursor and IR-induced fragment ions in a series of mass spectra recorded after irradiation at different wavelengths.

Over the past decade, IRIS has been recognized as a valuable method in structural elucidation in ion chemistry (for recent reviews, see, for example, refs 1−3). More recently, analytical applications of IRIS have been reported, demonstrating especially its potential in molecular structure identification in (un)targeted MS applications, in a range of fields such as glycomics,[4−6] synthetic chemistry,[7−10] environmental science,[11] pharmaceutical science,[12,13] and clinical chemistry.[14,15] Identification of individual metabolites embedded in biological matrices such as urine, plasma, and cerebrospinal fluid,[1,14,15] with or without chromatographic separation,[1,12,16] is a particularly appealing and innovative aspect of this methodology.

In the domain of forensic sciences, IRIS was employed to identify the precise isomeric form of novel psychoactive substances (NPSs) in confiscated samples,[17] to study the spectral characteristics of ecstasy and its metabolites,[18] and to structurally elucidate the $MS^n$ product ions of synthetic cathinones.[19] Here, we apply IRIS for the identification of individual NPSs in forensic samples containing isomeric mixtures, without using chromatographic separation.

As an MS-based method, IRIS analysis of samples containing isomeric species is often challenging. Note that we will use the term isomers to indicate not only constitutional isomers but also tautomers, diastereomers, conformers, etc. An IRIS spectrum recorded for a population of mass-selected ions that corresponds to multiple isomeric species results in a composite of the individual IR spectra, unless the isomers have distinct dissociation MS/MS spectra that can be used to generate unique IR spectra. An effective IRIS-based method to determine whether multiple isomers are present in the ion population is to perform an isomer population analysis experiment.[20−25] For spectroscopically distinguishable ion populations, the IR-resonant and nonresonant ion populations dissociate at different rates, which can be monitored by changing the IR irradiation time. From measurements of the

**Received:** December 1, 2020
**Accepted:** January 12, 2021
**Published:** January 20, 2021

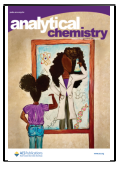





https://dx.doi.org/10.1021/acs.analchem.0c05042
*Anal. Chem.* 2021, 93, 2687−2693

on-resonance kinetics (i.e., precursor ion depletion as a function of the number of IR laser pulses) at a frequency diagnostic for a single isomer and at a frequency common to all isomers, the relative abundances of isomeric species in the ion population can be derived.

In cases where two isomeric species produce fragment ions of distinct $m/z$ upon IR dissociation, the IR spectra of the individual isomeric species can be reconstructed from the dissociation yields into the different fragment ion channels as a function of IR frequency.[26] Alternatively, liquid chromatography[1,4,12] or ion mobility[27−29] have been employed to separate isomeric species prior to IRIS analysis. If the isomers are spectroscopically distinguishable, which can be assessed from an isomer population analysis, two-color IR double-resonance spectroscopic schemes can be applied to record their individual IR spectra.[30−34]

Most isomer-selective IR−IR double-resonance schemes for ion spectroscopy reported to date include three stages of mass-to-charge ion selection with two IR laser interaction regions, and are therefore often denoted as $IR^2MS^3$. In the first MS stage, the $m/z$ of the precursor ion of interest is isolated, followed by irradiation with the first IR laser at frequency $\nu_1$. In a conventional IRIS experiment, one would then record a mass spectrum to detect the IR-induced fragment ions and repeat at different wavelengths to reconstruct an IR photodissociation spectrum; this method can therefore be referred to as $IRMS^2$. In $IR^2MS^3$, the $\nu_1$-induced fragment ions are removed in the second MS stage, leaving behind the nondissociated precursor ions, i.e., the isomer that does not absorb at $\nu_1$. These ions are then irradiated with the second IR laser at a frequency $\nu_2$ and the third MS stage records the $\nu_2$-induced fragment mass spectrum.

These $IR^2MS^3$ schemes were first demonstrated on custom-built MS setups with cryogenic ion traps. A weakly bound "tag" (rare gas atoms, $H_2$, $D_2$, or $N_2$) is attached to the precursor ions to deploy IR predissociation spectroscopy to record the IR spectrum of the tagged precursor ion.[30−33] Two IR lasers are used together with one[31,32] or two[30,33] laser interaction regions, and the MS stages are physically separated (often time-of-flight mass spectrometers). Furthermore, this method exploits a fixed $\nu_2$ frequency (probe) monitoring one specific isomer population, while $\nu_1$ is scanned.[30−33] This provides the IR spectrum of isomers having an absorption band at $\nu_2$. Alternatively, the $\nu_1$ laser frequency can be fixed to remove ("burn away") all isomers having absorption at $\nu_1$ while scanning $\nu_2$ to provide the IR spectrum of the other isomer.[33,34]

Cryogenically cooled ion trap mass spectrometers are not commercially available, in contrast to "regular" quadrupole ion trap mass spectrometers. These instruments feature extensive $MS^n$ capabilities, and optical access to the trapped ion population can be implemented (and is even commercially available on some platforms) to perform $IRMS^2$ experiments, for which various wavelength-tunable IR lasers have been employed.[4,35−39] Since IR predissociation spectroscopy on tagged ions is not possible at room temperature, IR multiple-photon dissociation (IRMPD) spectroscopy is used instead. The flexibility with which $MS^n$ parameters can be adjusted on these instruments makes $IRMS^2$ and population analysis experiments relatively facile to perform. From a mass spectrometric standpoint, an $IR^2MS^3$ experiment is also straightforward to implement, as it is strictly an $MS^3$ experiment. However, since there is only a single laser interaction region, i.e., the center of the three-dimensional (3D) quadrupole ion trap, the optical alignment of two (counter-propagating) laser beams is challenging, although a few examples have been reported.[34,36,39] In this contribution, we show that it is also possible to perform $IR^2MS^3$ measurements with a single tunable IR laser. We illustrate the potential of these methods by identifying two unknown isomeric NPSs in a sample that was confiscated by the Amsterdam Police.

## EXPERIMENTAL SECTION

**Materials.** Methanol (LC−MS grade), water (LC−MS grade), and formic acid (LC−MS grade) were purchased from VWR (Leuven, Belgium). 2-Fluoromethamphetamine (2-FMA) and 4-fluoromethamphetamine (4-FMA) reference standards were obtained from Cayman Chemical Company (Ann Arbor, MI). The case sample was a seized street sample containing unidentified NPSs provided by the Amsterdam Police Laboratory.

**Infrared Ion Spectroscopy ($IRMS^2$).** IRIS measurements were performed using a commercial 3D quadrupole ion trap mass spectrometer with optical access to the ion trapping region (Bruker amaZon speed ETD).[35] The ion trap was operated in the positive electrospray ionization-mass spectrometry (ESI-MS) mode and the sample solution was infused at a 3 $\mu$L/min flow rate. In the ion trapping region, mass-to-charge ($m/z$) selected ions were irradiated by a single infrared laser pulse from the Free Electron Laser for Infrared eXperiments (FELIX) to induce wavelength-dependent infrared multiple-photon dissociation (IRMPD).[1,40] FELIX was operated at 10 Hz with a pulse energy of ∼100 mJ in the frequency range of 600−1800 $cm^{-1}$. In the MS sequence of the ion trap, IR photodissociation is achieved by defining an MS/MS window with an excitation amplitude of zero that serves as the IRMPD window. A window of 80 ms was chosen to ensure that the ion population is irradiated by a single IR laser pulse. Full details on triggering and synchronization are reported elsewhere.[35] The IR spectra of $m/z$-selected ions are obtained by plotting the IRMPD yield as a function of IR frequency. The IRMPD yield is defined as the ratio of the sum of all fragment ions over the sum of all ions (fragments + precursor) and is obtained from six averaged mass spectra for each IR wavelength. The IR frequency was calibrated online using a grating spectrometer, and the yield was linearly corrected for variations in the IR pulse energy.[40] Recording an IR spectrum over the 600−1800 $cm^{-1}$ spectral range takes about 25 min, of which about 50% is needed for stepping the FEL undulator gap to change the IR frequency (in 3 $cm^{-1}$ intervals).[41]

**Isomer Population Analysis.** To determine whether multiple isomeric species are present in the $m/z$-selected ion population, a population analysis experiment can be performed. The laser is parked at a fixed IR frequency and the duration of the IRMPD window is increased in steps of 100 ms so that the ion population is irradiated with an increasing number of laser pulses. Plotting the normalized precursor ion intensity (which is equal to 1 − yield) as a function of the number of laser pulses generates a precursor ion depletion curve. If the precursor ion intensity does not converge to zero for a large number of pulses, multiple (isobaric) species are likely present in the ion population. Recording a precursor ion depletion curve takes $\sum_{i=0}^{K}(i \times \Delta t + t_{ms})$ seconds, where $K$ is the maximum number of laser pulses, $\Delta t$ is the time between laser pulses (here 0.1 s), and $t_{ms}$ is the duration of a single MS


https://dx.doi.org/10.1021/acs.analchem.0c05042
Anal. Chem. 2021, 93, 2687−2693

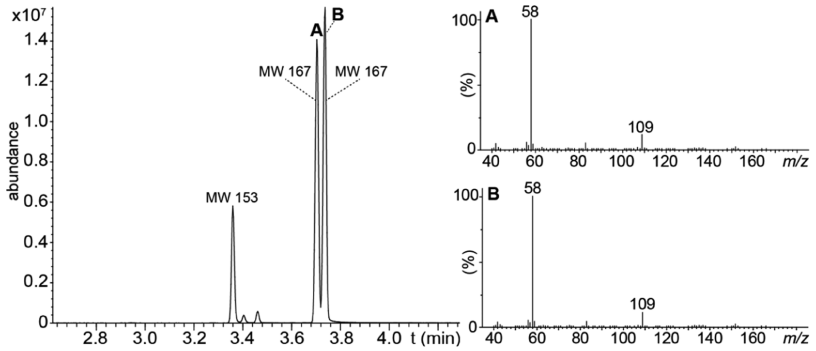


**Figure 1.** GC−MS chromatogram of the case sample and electron ionization (EI) mass spectra from the chromatographic peaks labeled A and B. A mass spectral library search indicates that A and B both have MW 167. Details on the GC−MS analysis are provided in the Supporting Information.

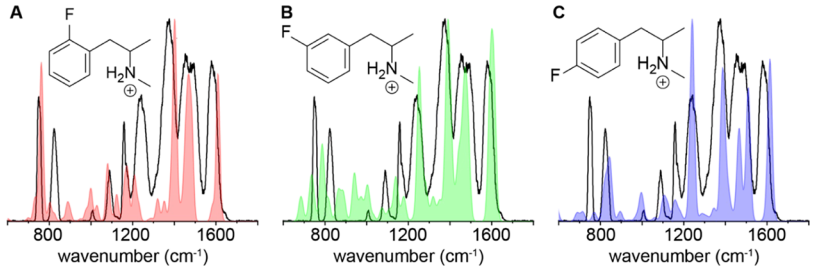


**Figure 2.** Experimental IRIS spectrum of the $m/z$ 168 ion from the case sample (black trace in all panels) compared with computationally predicted spectra of protonated FMA in its three isomeric forms: (A) 2-FMA (red), (B) 3-FMA (green), and (C) 4-FMA (blue).

sequence (accumulation, isolation, scanning the mass spectrum), which is in our case <0.1 s. With $K$ = 20, a depletion curve is measured in less than 30 s.

**Two-Color IR−IR Double-Resonance Spectroscopy ($IR^2MS^3$).** From the precursor ion depletion curves that do not converge to zero for a large number of laser pulses, the number of IR laser pulses ($N$) needed to dissociate all ions absorbing at that particular IR frequency, $\nu_{burn}$, can be read off. An $IR^2MS^3$ experiment is then performed as follows: (1) the IR frequency is tuned to $\nu_{burn}$, and the $m/z$-selected precursor ions are irradiated with $N$ pulses to burn away all ions absorbing at that IR frequency; (2) the remaining precursor ions are $m/z$ isolated removing all IR-induced fragment ions produced in step (1) from the trap; (3) the $m/z$-selected ions remain trapped during a waiting time in the MS sequence to allow the IR laser frequency to be tuned to a new, scanned frequency, $\nu_{scan}$; (4) the remaining precursor ions are irradiated with a single IR laser pulse at $\nu_{scan}$; and (5) a mass spectrum is recorded and the IR dissociation yield is determined as in conventional $IRMS^2$ spectroscopy. This 5-step process is repeated, keeping the $\nu_{burn}$ fixed and scanning $\nu_{scan}$ in typically 5 $cm^{-1}$ intervals over the desired scan range, thus recording the IR spectrum of the nonburned isomer(s).

Obviously, an $IR^2MS^3$ measurement requires more time than a regular $IRMS^2$ scan because the IR laser frequency tunes back-and-forth between $\nu_{burn}$ and $\nu_{scan}$ and, in addition, the laser irradiates the trapped ions with $N$ laser pulses at $\nu_{burn}$ versus only a single laser pulse at $\nu_{scan}$. An $IR^2MS^3$ measurement with a scan range of 600−1800 $cm^{-1}$, a $\nu_{burn}$ of around 1200 $cm^{-1}$ (in the middle of the scan range), and $N$ = 15 takes about 90 min in our setup, where the largest fraction of this time is spent on changing the FELIX wavelength. Many laboratories use tabletop IR lasers to perform IRMPD spectroscopy in the hydrogen stretching range that can be tuned much faster,[4,30−33,35−39] which would greatly reduce the time required for an $IR^2MS^3$ spectrum.

All experiments, regular IRIS ($IRMS^2$), isomer population analysis, and double-resonance IRIS ($IR^2MS^3$), are fully automated by controlling and storing all MS, MS/MS, and laser parameters in Bruker Compass software using an XML scripting interface within an in-house designed LabView program.[35]

**Computational Methods.** Geometries of the drug molecules were optimized at the B3LYP/6-31++G(d,p) level of theory using the Gaussian16 software package.[42] Harmonic vibrational frequencies were computed for each optimized geometry and were scaled by a factor 0.975 and broadened with a 25 $cm^{-1}$ full width at half-maximum (FWHM) Gaussian line shape to facilitate comparison with the experimental spectra.

## RESULTS AND DISCUSSION

**Infrared Ion Spectroscopy of a Sample Containing Isomeric Compounds.** To demonstrate the capabilities of the combination of the three experimental techniques $IRMS^2$, isomer population analysis, and $IR^2MS^3$, we analyzed a case sample containing isomeric NPSs. First, an exploratory GC−MS analysis was performed in the Police Laboratory to obtain an indication of the identity of the compounds and their quantities. Figure 1 shows the acquired chromatogram of the sample, as well as EI-MS spectra of the chromatographic peaks, labeled A and B. Given the almost identical EI-MS spectra, the closeness of the two GC peaks, and the results of the mass spectral library search, the sample likely contains two fluoromethamphetamine isomers having a molecular weight (MW) of 167 (see Tables S1 and S2).

An $IRMS^2$ analysis was performed on the mixture of isomeric compounds from the case sample ($ESI^+$, $m/z$ 168 as $[M + H]^+$). On-resonance IRMPD gave two fragment ions


https://dx.doi.org/10.1021/acs.analchem.0c05042
Anal. Chem. 2021, 93, 2687−2693

with $m/z$ 137 (likely the neutral loss of methylamine) and 109 (likely the neutral loss of ethylmethylamine). The IR spectrum obtained for $m/z$ 168 is shown in Figure 2 along with computationally predicted IR spectra for three ring-substituent positional isomers of fluoromethamphetamine (FMA), i.e., the structures suggested by the GC−MS spectral library. Although the density functional theory (DFT) computed spectra generally provide a reasonably good match with experimental IRIS spectra for small molecules, which often gives a reliable molecular structure assignment,[16−18] this is not the case here: none of the calculated spectra convincingly matches the experimental IRIS spectrum. This may imply that the case sample contains a mixture of MW 167 isomers. With this hypothesis in mind and careful inspection of the spectra in Figure 2, one may estimate which of the isomers are actually present, especially from the 650−900 $cm^{-1}$ region where ortho-, meta-, and para-isomers have distinct spectral signatures, originating from the out-of-plane CH-bending vibrations of the aromatic ring.[17,43] This suggests that 2-FMA (ortho) and 4-FMA (para) are present in the case sample.

**Isomer Population Analysis.** To determine the number of $m/z$ 168 isomers present in the ESI mass spectrum of the sample, as well as their relative abundances, an isomer population analysis was performed at the seven bands labeled 1−7 in Figure 3A. The corresponding precursor ion depletion curves are shown in panels 1−7 of Figure 3. To illustrate the power of an isomer population analysis and to fully understand all precursor ion depletion curves, we have recorded the IRIS spectra of protonated 2-FMA and 4-FMA from reference standards (Figure 3B,C).

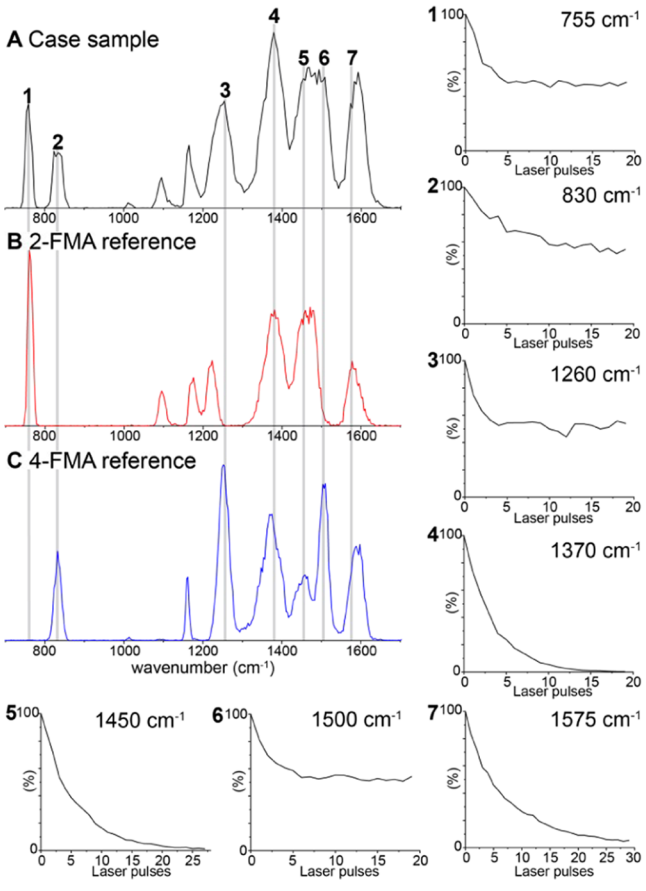


**Figure 3.** IRIS spectra of the case sample (A) and the 2-FMA (B) and 4-FMA (C) reference compounds, and isomer population analysis curves at seven vibrational bands (1−7).

At 1370 $cm^{-1}$ (label 4), all ions have undergone dissociation after 15 laser pulses, indicating that all $m/z$ 168 ions absorb at this IR frequency (and that all trapped ions have spatial overlap with the laser focus). In contrast, for bands 1, 2, 3, and 6, the precursor ion depletion converges to a plateau at ∼50% after 5−20 laser pulses, indicating the presence of multiple isobaric species. Finally, the precursor ion depletion curves measured at 1450 and 1575 $cm^{-1}$ (5 and 7) approach zero at 30 or more IR laser pulses, indicating that all isomers absorb at these frequencies. In comparison to excitation at 1370 $cm^{-1}$ (4), the "decay half-lives" at 5 and 7 are relatively long as a consequence of the lower absorption cross sections at these frequencies.

If we assume that only 2-FMA and 4-FMA are present in the mixture, the precursor ion depletion curves indicate that half of the ion population is 2-FMA and the other half is 4-FMA. Assuming, furthermore, that 2-FMA and 4-FMA have similar ESI ionization efficiencies, we may conclude that the ratio of 2-FMA to 4-FMA in the case sample is about 1:1, which agrees with their GC−MS chromatographic peak areas (Figure 1).

**IR−IR Double Resonance IRIS ($IR^2MS^3$) with a Single Laser.** $IR^2MS^3$ experiments were performed to disentangle the IR spectra of the individual isomers from the composite spectrum shown in Figure 3A. The precursor depletion curve 2 in Figure 3 shows that about 15 IR laser pulses at 830 $cm^{-1}$ are required to remove the 4-FMA isomer from the ion population, leaving only 2-FMA ions in the trap. Vice versa, around 15 IR pulses at 755 $cm^{-1}$ are required to remove all 2-FMA ions, leaving only 4-FMA ions in the trap. This allows one to record a "clean" IR spectrum of the remaining ions using the $IR^2MS^3$ approach, as illustrated for the 710−870 $cm^{-1}$ spectral range in Figure 4. Indeed, if we burn away the 4-FMA ions (Figure 4A), the resulting $IR^2MS^3$ spectrum is that of 2-FMA (Figure 4C). Similarly, if we burn away all 2-FMA ions (Figure 4B), the resulting spectrum is that of 4-FMA (Figure 4D).

A comparison of the absolute values of the yield in Figure 4 also provides the ratio of 2-FMA to 4-FMA ions. The yield in panels C and D is twice as high as the yield of the corresponding vibrational band in panels A and B, demonstrating that the ratio is 1:1 and thus nicely corresponds to the results obtained from the isomer population analysis.

The IR spectra shown in Figure 4 have been recorded by irradiating the ions with a single IR laser pulse at every IR frequency. Slow drift and pulse-to-pulse fluctuations of the IR laser pulse energy have an effect on the value of the yield, which explains the small discrepancies in intensities of the IR spectra in Figure 4. Variations in the laser pulse energy have no effect on the "burn" step in the $IR^2MS^3$ experiment since the number of pulses is large enough to ensure that all ions of the selected isomer are dissociated.

The complete individual IR spectra of both isomers from the case sample have also been recovered in a single $IR^2MS^3$ experiment. Here, we used another IR frequency to uniquely burn away the 4-FMA ions, 1260 $cm^{-1}$ (frequency 3 in Figure 3), to illustrate that the IR burn frequency is not critical as long as it is not resonant with an absorption in protonated 2-FMA. Figure 5A shows the $IRMS^2$ spectrum of $m/z$ 168 from the case sample, while the $IR^2MS^3$ spectrum of the remaining 2-FMA ions is displayed as a black trace in Figure 5B. The


https://dx.doi.org/10.1021/acs.analchem.0c05042
Anal. Chem. 2021, 93, 2687−2693

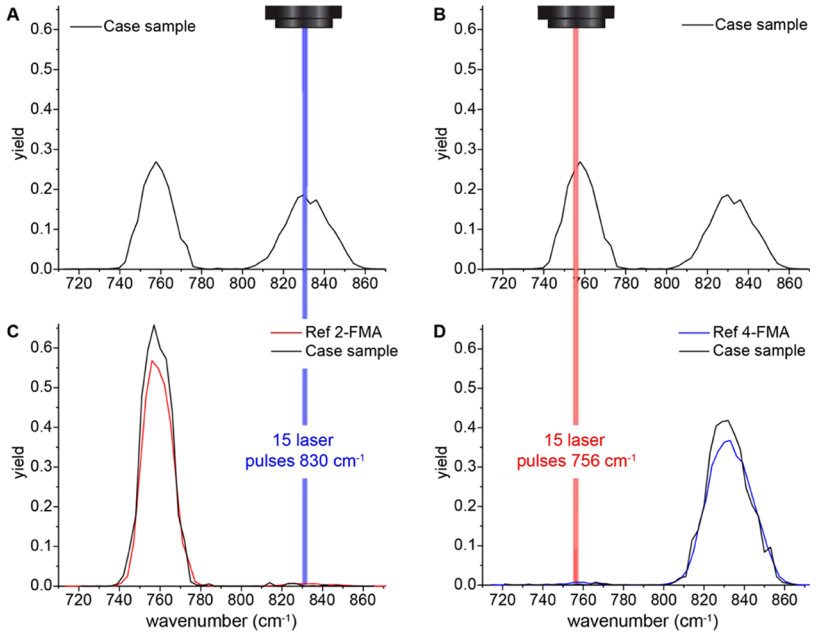


**Figure 4.** Principle of $IR^2MS^3$. Panels (A) and (B) show a part of the $IRMS^2$ spectrum of the case sample also displayed in Figure 3A. Panel (C) shows the $IR^2MS^3$ spectrum (black line) of the case sample obtained after burning away the 4-FMA ions at 830 $cm^{-1}$; the $IRMS^2$ spectrum of the 2-FMA reference compound is overlaid in red. Vice versa, panel (D) shows the $IR^2MS^3$ spectrum (black line) of the case sample obtained after burning away the 2-FMA ions at 756 $cm^{-1}$, and overlaid in blue the $IRMS^2$ spectrum of the 4-FMA reference compound. Note that these experiments involved only a single IR laser.

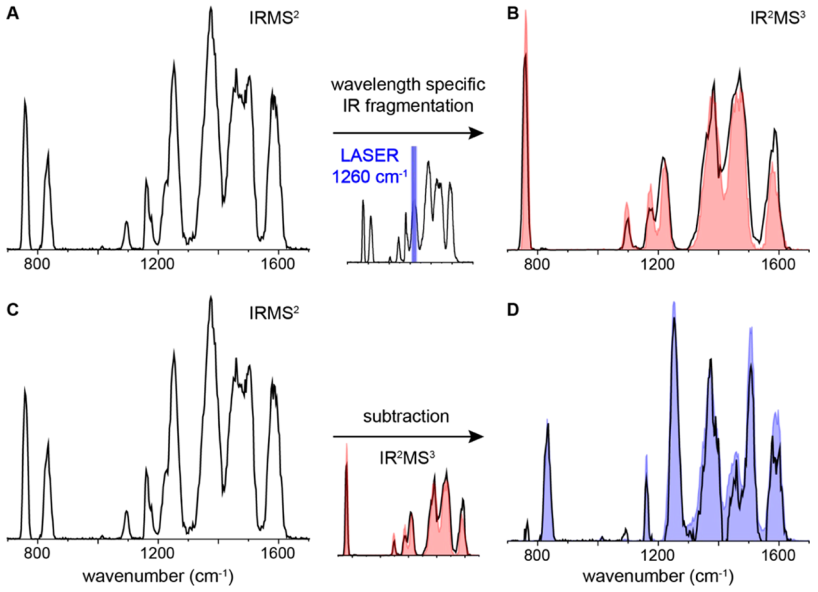


**Figure 5.** $IR^2MS^3$ experiment. The spectrum in panels (A) and (C) is the $IRMS^2$ spectrum of $m/z$ 168 from the case sample. Panel (B) shows the IRMPD spectrum of $m/z$ 168 with all 4-FMA ions burnt away at an IR frequency of 1260 $cm^{-1}$ (frequency 3 in Figure 3). Overlaid in red is the experimental IRMPD spectrum of the 2-FMA reference. Subtraction of the $IR^2MS^3$ spectrum (black trace B) from the $IRMS^2$ spectrum in (C) (multiplied by a factor of 2 to account for the presence of two species, as discussed in the text) gives the IR spectrum shown in panel (D) (black trace) and should correspond to the spectrum of 4-FMA. The blue overlay in (D) is the experimental IRMPD spectrum of the protonated 4-FMA reference.

spectrum of the 2-FMA reference compound is overlaid in red, demonstrating that all spectral features in the case sample $IR^2MS^3$ spectrum can indeed be attributed to 2-FMA.

While the IR spectrum of the other isomer (4-FMA) can be obtained by performing a second $IR^2MS^3$ experiment burning away all 2-FMA ions, the IR spectrum of this isomer can also be derived from directly subtracting the $IR^2MS^3$ spectrum of 2-FMA from the sample $IRMS^2$ spectrum. Note that the $IRMS^2$ spectrum is multiplied by a factor of 2 to account for the presence of two species, as discussed above. The resulting "synthetic" spectrum, presented as the black line in Figure 5D, should correspond to that of 4-FMA. The somewhat poorer signal-to-noise ratio of this spectrum is due to imperfections in the subtraction, as is, for instance, visible around 756 $cm^{-1}$, where a slightly different spectral width and intensity does not cancel the 2-FMA band completely. Nevertheless, the


https://dx.doi.org/10.1021/acs.analchem.0c05042
Anal. Chem. 2021, 93, 2687−2693

spectrum obtained by subtraction shows a close overlap with the 4-FMA reference spectrum. Since all spectral features in the $IRMS^2$ spectrum can be attributed to vibrational bands belonging to either 2-FMA or 4-FMA, we conclude that the *m/z* 168 ion from the case sample is solely produced by protonated 2-FMA and 4-FMA and that there are no additional isomeric species present in the sample.

## CONCLUSIONS

We have shown that an optically accessible quadrupole ion trap mass spectrometer coupled to a wavelength-tunable IR laser can be employed for two-color double resonance ($IR^2MS^3$) spectroscopic measurements, using only a single laser source. The method has been fully automated making use of the $MS^n$ functionalities of the Bruker amaZon mass spectrometer. The capability of an ion trap to keep the ions trapped for an arbitrary time allows the use of a single laser to perform two-color $IR^2MS^3$ experiments, where one IR frequency is used to remove one isomer from the trapped ion population and the second IR frequency records the spectrum of the remaining "precursor" ions. The $IR^2MS^3$ experiments were combined with population analysis measurements, in which the IR irradiation time is varied at specific fixed IR frequencies to record the precursor ion depletion as a function of the number of laser pulses. This reveals the number of isomeric species and their relative abundances.

The arsenal of three IR ion spectroscopy tools, $IRMS^2$, isomer population analysis, and $IR^2MS^3$, has been applied to a forensic case sample containing isomeric NPSs. Two analytes with MW 167 were identified as 2-FMA and 4-FMA, present in an approximately 1:1 ratio. For the purpose of demonstrating the $IRMS^2$, isomer population analysis and $IR^2MS^3$ methods and evaluating their performance and validity, we have made use of the availability of reference standards of the 2-FMA and 4-FMA isomers. However, in cases where reference standards are not available, the methods can be applied using DFT-computed reference spectra instead, expanding the potential of IRIS-based identification to true unknowns.

Beyond the application of an IR FEL demonstrated in this work, the extended IRIS toolbox is especially useful for ion trap mass spectrometers connected to table-top IR lasers, which are used by various labs for ion spectroscopy and analysis of complex mixtures.[4,35−39] The combination of a commercial quadrupole ion trap mass spectrometer with a single IR laser provides a simple and cost-effective way to perform $IRMS^2$, isomer population analysis, and $IR^2MS^3$ experiments. Moreover, the faster frequency tuning capabilities of the current commercial IR laser systems, as compared to an FEL, make the application of $IR^2MS^3$ especially attractive on these systems. Apart from application in forensic sciences, as shown here, applications are envisioned in environmental, pharmaceutical, and (bio)analytical sciences.

## ASSOCIATED CONTENT

### Supporting Information

The Supporting Information is available free of charge at https://pubs.acs.org/doi/10.1021/acs.analchem.0c05042.

GC−MS analysis method and MS library search results for peak A and B spectra in Figure 1 (PDF)

## AUTHOR INFORMATION


### Corresponding Author

**Giel Berden** − *FELIX Laboratory, Institute for Molecules and Materials, Radboud University, 6525 ED Nijmegen, The Netherlands;* orcid.org/0000-0003-1500-922X; Phone: +31 243653951; Email: g.berden@science.ru.nl

### Authors

**Fred A. M. G. van Geenen** − *FELIX Laboratory, Institute for Molecules and Materials, Radboud University, 6525 ED Nijmegen, The Netherlands;* orcid.org/0000-0002-4284-6333

**Ruben F. Kranenburg** − *Forensic Laboratory, Unit Amsterdam, Dutch National Police, 1014 BA Amsterdam, The Netherlands; Van't Hoff Institute for Molecular Sciences, University of Amsterdam, 1090 GD Amsterdam, The Netherlands;* orcid.org/0000-0003-1472-3739

**Arian C. van Asten** − *Van't Hoff Institute for Molecular Sciences, University of Amsterdam, 1090 GD Amsterdam, The Netherlands; Co van Ledden Hulsebosch Center (CLHC), Amsterdam Center for Forensic Science and Medicine, 1090 GD Amsterdam, The Netherlands*

**Jonathan Martens** − *FELIX Laboratory, Institute for Molecules and Materials, Radboud University, 6525 ED Nijmegen, The Netherlands;* orcid.org/0000-0001-9537-4117

**Jos Oomens** − *FELIX Laboratory, Institute for Molecules and Materials, Radboud University, 6525 ED Nijmegen, The Netherlands; Van't Hoff Institute for Molecular Sciences, University of Amsterdam, 1090 GD Amsterdam, The Netherlands;* orcid.org/0000-0002-2717-1278

Complete contact information is available at: https://pubs.acs.org/10.1021/acs.analchem.0c05042

### Author Contributions

⊥F.A.M.G.v.G. and R.F.K. contributed equally to this manuscript.


### Notes

The authors declare no competing financial interest.

## ACKNOWLEDGMENTS

Guus Tielemans is acknowledged for his excellent help and assistance in software development. The authors are grateful to receive funding for this research from the Radboud University through an interfaculty collaboration grant, the Netherlands Organization for Scientific Research (NWO) for their support of the FELIX Laboratory [Grant Numbers VICI 724.011.002, TTW 15769], and SURFsara for computational resources [NWO Rekentijd Grant 2019.062].

## REFERENCES


(1) Martens, J.; van Outersterp, R. E.; Vreeken, R. J.; Cuyckens, F.; Coene, K. L. M.; Engelke, U. F.; Kluijtmans, L. A. J.; Wevers, R. A.; Buydens, L. M. C.; Redlich, B.; Berden, G.; Oomens, J. *Anal. Chim. Acta* **2020**, *1093*, 1−15.

(2) Jašíková, L.; Roithová, J. *Chem. − Eur. J.* **2018**, *24*, 3374−3390.

(3) Maitre, P.; Scuderi, D.; Corinti, D.; Chiavarino, B.; Crestoni, M. E.; Fornarini, S. *Chem. Rev.* **2020**, *120*, 3261−3295.

(4) Schindler, B.; Laloy-Borgna, G.; Barnes, L.; Allouche, A.-R.; Bouju, E.; Dugas, V.; Demesmay, C.; Compagnon, I. *Anal. Chem.* **2018**, *90*, 11741−11745.

(5) Dyukova, I.; Carrascosa, E.; Pellegrinelli, R. P.; Rizzo, T. R. *Anal. Chem.* **2020**, *92*, 1658−1662.

(6) Lettow, M.; Grabarics, M.; Greis, K.; Mucha, E.; Thomas, D. A.; Chopra, P.; Boons, G.-J.; Karlsson, R.; Turnbull, J. E.; Meijer, G.; Miller, R. L.; von Helden, G.; Pagel, K. *Anal. Chem.* **2020**, *92*, 10228−10232.
(7) Pahl, M.; Mayer, M.; Schneider, M.; Belder, D.; Asmis, K. R. *Anal. Chem.* **2019**, *91*, 3199−3203.
(8) Elferink, H.; Severijnen, M. E.; Martens, J.; Mensink, R. A.; Berden, G.; Oomens, J.; Rutjes, F. P. J. T.; Rijs, A. M.; Boltje, T. J. *J. Am. Chem. Soc.* **2018**, *140*, 6034−6038.
(9) Mucha, E.; Marianski, M.; Xu, F.-F.; Thomas, D. A.; Meijer, G.; von Helden, G.; Seeberger, P. H.; Pagel, K. *Nat. Commun.* **2018**, *9*, No. 4174.
(10) Dvores, M. P.; Çarçabal, P.; Maître, P.; Simons, J. P.; Gerber, R. B. *Phys. Chem. Chem. Phys.* **2020**, *22*, 4144−4157.
(11) Walhout, E. Q.; Dorn, S. E.; Martens, J.; Berden, G.; Oomens, J.; Cheong, P. H. Y.; Kroll, J. H.; O'Brien, R. E. *Environ. Sci. Technol.* **2019**, *53*, 7604−7612.
(12) Martens, J.; Koppen, V.; Berden, G.; Cuyckens, F.; Oomens, J. *Anal. Chem.* **2017**, *89*, 4359−4362.
(13) Lagatie, O.; Verheyen, A.; Van Asten, S.; Odiere, M. R.; Djuardi, Y.; Levecke, B.; Vlaminck, J.; Mekonnen, Z.; Dana, D.; T'Kindt, R.; Sandra, K.; van Outersterp, R.; Oomens, J.; Lin, R.; Dillen, L.; Vreeken, R.; Cuyckens, F.; Stuyver, L. J. *Sci. Rep.* **2020**, *10*, No. 15780.
(14) Martens, J.; Berden, G.; van Outersterp, R. E.; Kluijtmans, L. A. J.; Engelke, U. F.; van Karnebeek, C. D. M.; Wevers, R. A.; Oomens, J. *Sci. Rep.* **2017**, *7*, No. 3363.
(15) Martens, J.; Berden, G.; Bentlage, H.; Coene, K. L. M.; Engelke, U. F.; Wishart, D.; van Scherpenzeel, M.; Kluijtmans, L. A. J.; Wevers, R. A.; Oomens, J. *J. Inherited Metab. Dis.* **2018**, *41*, 367−377.
(16) van Outersterp, R. E.; Houthuijs, K. J.; Berden, G.; Engelke, U. F.; Kluijtmans, L. A. J.; Wevers, R. A.; Coene, K. L. M.; Oomens, J.; Martens, J. *Int. J. Mass Spectrom.* **2019**, *443*, 77−85.
(17) Kranenburg, R. F.; van Geenen, F. A. M. G.; Berden, G.; Oomens, J.; Martens, J.; van Asten, A. C. *Anal. Chem.* **2020**, *92*, 7282−7288.
(18) Bell, M. R.; Tesler, L. F.; Polfer, N. C. *Int. J. Mass Spectrom.* **2019**, *443*, 101−108.
(19) Davidson, J. T.; Piacentino, E. L.; Sasiene, Z. J.; Abiedalla, Y.; DeRuiter, J.; Clark, C. R.; Berden, G.; Oomens, J.; Ryzhov, V.; Jackson, G. P. *Forensic Chem.* **2020**, *19*, No. 100245.
(20) Prell, J. S.; Chang, T. M.; O'Brien, J. T.; Williams, E. R. *J. Am. Chem. Soc.* **2010**, *132*, 7811−7819.
(21) Prell, J. S.; Chang, T. M.; Biles, J. A.; Berden, G.; Oomens, J.; Williams, E. R. *J. Phys. Chem. A* **2011**, *115*, 2745−2751.
(22) Munshi, M. U.; Martens, J.; Berden, G.; Oomens, J. *J. Phys. Chem. A* **2019**, *123*, 8226−8233.
(23) Patrick, A. L.; Cismesia, A. P.; Tesler, L. F.; Polfer, N. C. *Int. J. Mass Spectrom.* **2017**, *418*, 148−155.
(24) Chiavarino, B.; Crestoni, M. E.; Fornarini, S.; Scuderi, D.; Salpin, J.-Y. *Inorg. Chem.* **2017**, *56*, 8793−8801.
(25) Paciotti, R.; Corinti, D.; De Petris, A.; Ciavardini, A.; Piccirillo, S.; Coletti, C.; Re, N.; Maitre, P.; Bellina, B.; Barran, P.; Chiavarino, B.; Elisa Crestoni, M.; Fornarini, S. *Phys. Chem. Chem. Phys.* **2017**, *19*, 26697−26707.
(26) Kempkes, L. J. M.; Martens, J.; Berden, G.; Oomens, J. *Int. J. Mass Spectrom.* **2018**, *429*, 90−100.
(27) Ben Faleh, A.; Warnke, S.; Rizzo, T. R. *Anal. Chem.* **2019**, *91*, 4876−4882.
(28) Warnke, S.; Seo, J.; Boschmans, J.; Sobott, F.; Scrivens, J. H.; Bleiholder, C.; Bowers, M. T.; Gewinner, S.; Schöllkopf, W.; Pagel, K.; von Helden, G. *J. Am. Chem. Soc.* **2015**, *137*, 4236−4242.
(29) Hernandez, O.; Isenberg, S.; Steinmetz, V.; Glish, G. L.; Maitre, P. *J. Phys. Chem. A* **2015**, *119*, 6057−6064.
(30) Elliott, B. M.; Relph, R. A.; Roscioli, J. R.; Bopp, J. C.; Gardenier, G. H.; Guasco, T. L.; Johnson, M. A. *J. Chem. Phys.* **2008**, *129*, No. 094303.
(31) Heine, N.; Fagiani, M. R.; Rossi, M.; Wende, T.; Berden, G.; Blum, V.; Asmis, K. R. *J. Am. Chem. Soc.* **2013**, *135*, 8266−8273.
(32) Jašík, J.; Gerlich, D.; Roithová, J. *J. Phys. Chem. A* **2015**, *119*, 2532−2542.
(33) Voss, J. M.; Kregel, S. J.; Fischer, K. C.; Garand, E. *J. Am. Soc. Mass Spectrom.* **2018**, *29*, 42−50.
(34) Schäfer, M.; Peckelsen, K.; Paul, M.; Martens, J.; Oomens, J.; Berden, G.; Berkessel, A.; Meijer, A. J. H. M. *J. Am. Chem. Soc.* **2017**, *139*, 5779−5786.
(35) Martens, J.; Berden, G.; Gebhardt, C. R.; Oomens, J. *Rev. Sci. Instrum.* **2016**, *87*, No. 103108.
(36) Nosenko, Y.; Menges, F.; Riehn, C.; Niedner-Schatteburg, G. *Phys. Chem. Chem. Phys.* **2013**, *15*, 8171−8178.
(37) Aleese, L. M.; Simon, A.; McMahon, T. B.; Ortega, J.-M.; Scuderi, D.; Lemaire, J.; Maître, P. *Int. J. Mass Spectrom.* **2006**, *249*−*250*, 14−20.
(38) Hamlow, L. A.; Zhu, Y.; Devereaux, Z. J.; Cunningham, N. A.; Berden, G.; Oomens, J.; Rodgers, M. T. *J. Am. Soc. Mass Spectrom.* **2018**, *29*, 2125−2137.
(39) Penna, T. C.; Cervi, G.; Rodrigues-Oliveira, A. F.; Yamada, B. D.; Lima, R. Z. C.; Menegon, J. J.; Bastos, E. L.; Correra, T. C. *Rapid Commun. Mass Spectrom.* **2020**, *34*, No. e8635.
(40) Berden, G.; Derksen, M.; Houthuijs, K. J.; Martens, J.; Oomens, J. *Int. J. Mass Spectrom.* **2019**, *443*, 1−8.
(41) Oepts, D.; van der Meer, A. F. G.; van Amersfoort, P. W. *Infrared Phys. Technol.* **1995**, *36*, 297−308.
(42) Frisch, M. J.; Trucks, G. W.; Schlegel, H. B.; Scuseria, G. E.; Robb, M. A.; Cheeseman, J. R.; Scalmani, G.; Barone, V.; Petersson, G. A.; Nakatsuji, H.; Li, X.; Caricato, M.; Marenich, A. V.; Bloino, J.; Janesko, B. G.; Gomperts, R.; Mennucci, B.; Hratchian, H. P.; Ortiz, J. V.; Izmaylov, A. F.; Sonnenberg, J. L.; Williams; Ding, F.; Lipparini, F.; Egidi, F.; Goings, J.; Peng, B.; Petrone, A.; Henderson, T.; Ranasinghe, D.; Zakrzewski, V. G.; Gao, J.; Rega, N.; Zheng, G.; Liang, W.; Hada, M.; Ehara, M.; Toyota, K.; Fukuda, R.; Hasegawa, J.; Ishida, M.; Nakajima, T.; Honda, Y.; Kitao, O.; Nakai, H.; Vreven, T.; Throssell, K.; Montgomery, J. A., Jr.; Peralta, J. E.; Ogliaro, F.; Bearpark, M. J.; Heyd, J. J.; Brothers, E. N.; Kudin, K. N.; Staroverov, V. N.; Keith, T. A.; Kobayashi, R.; Normand, J.; Raghavachari, K.; Rendell, A. P.; Burant, J. C.; Iyengar, S. S.; Tomasi, J.; Cossi, M.; Millam, J. M.; Klene, M.; Adamo, C.; Cammi, R.; Ochterski, J. W.; Martin, R. L.; Morokuma, K.; Farkas, O.; Foresman, J. B.; Fox, D. J.. *Gaussian 16*; Gaussian Inc.: Wallingford, CT, 2016.
(43) van Outersterp, R. E.; Martens, J.; Berden, G.; Koppen, V.; Cuyckens, F.; Oomens, J. *Analyst* **2020**, *145*, 6162−6170.


https://dx.doi.org/10.1021/acs.analchem.0c05042
*Anal. Chem.* 2021, 93, 2687−2693